Polarization rotation, switching, and electric-field–temperature phase diagrams of ferroelectric $BaTiO_3$: A molecular dynamics study

Jaita Paul,[1] Takeshi Nishimatsu,[2] Yoshiyuki Kawazoe,[2] and Umesh V. Waghmare[1]
[1]*TSU, Jawaharlal Nehru Centre for Advanced Scientific Research, Jakkur P.O., Bangalore 560 064, India*
[2]*Institute for Materials Research, Tohoku University, Sendai 980-8577, Japan*
(Received 12 August 2008; revised manuscript received 30 April 2009; published 10 July 2009)

We use molecular dynamics simulations to understand the mechanisms of polarization switching in ferroelectric $BaTiO_3$ achieved with external electric field. For tetragonal and orthorhombic ferroelectric phases, we determine the switching paths and show that polarization rotation through intermediate monoclinic phases (a) facilitates switching at low fields and (b) is responsible for a sharp anisotropy in polarization switching. We develop an understanding of this through the determination of detailed electric-field–temperature phase diagrams that are fundamental to technological applications based on electromechanical and switching response of ferroelectrics.

DOI: 10.1103/PhysRevB.80.024107 PACS number(s): 77.80.Fm, 64.60.Ej, 77.80.Bh, 77.84.Dy

I. INTRODUCTION

Ferroelectric (FE) materials exhibit spontaneous electric polarization whose magnitude and direction depend sensitively on temperature, pressure, and electric field.[1] They are technologically very important because of two of their properties: (a) large electromechanical coupling that is exploited in their applications as sensors and actuators in microelectromechanical systems[1] and (b) switchability of their polarization from one state to another with applied field that makes them useful in nonvolatile memory devices such as ferroelectric random access memories (FeRAMs).[2] Fundamental understanding of the mechanisms responsible for these properties in the bulk crystals is essential to the development of ferroelectrics with improved properties and their use in nanoscale devices.

The direction of spontaneous polarization is typically along a crystallographic direction. Polarization rotation[3] from a rhombohedral state toward a tetragonal one through an intermediate monoclinic phase was shown to be responsible for an ultrahigh piezoelectric coupling observed experimentally.[4] Monoclinic phases, characterized by the polarization vector (**P**) along low-symmetry directions, were carefully analyzed and shown to be relevant to the large piezoelectricity in $92\%PbZn_{1/3}Nb_{2/3}O_3$-$8\%PbTiO_3$ (Ref. 5) and also found in another technologically important ferroelectric $Pb(Zr_xTi_{1-x})O_3$.[6]

Interestingly, piezoelectric response of $BaTiO_3$ (a simple classic ferroelectric) was shown to be enhanced significantly by crystallographically engineering single crystals through applied dc bias.[7,8] This involves the nonlinear response of $BaTiO_3$ and is linked with electric-field-induced structural phase transitions[4,5,9] in ferroelectrics. Polarization switching, crucial to memory applications, is another closely related nonlinear phenomenon whose microscopic mechanism is yet to be uncovered. Understanding of these nonlinear phenomena within a single picture is facilitated by the knowledge of electric-field–temperature phase diagrams of a ferroelectric.

Using phenomenological the Landau-Ginzburg-Devonshire theory, electric-field–temperature (E-T) phase diagrams have been studied for single-crystal $BaTiO_3$, showing evidence for monoclinic phases.[10] Similarly, it was shown in general by Vanderbilt and Cohen[11] that the extension of the sixth-order Devonshire theory to the eighth and twelfth orders in polarization as the order parameter was necessary to explain the presence of stable monoclinic and triclinic phases, respectively.

In this work we define polarization switching as follows: *for an electric field* **E** applied along the $\hat{\mathbf{e}}$ direction and cycled between E_{max} and $-E_{max}$, polarization is switched when $(\mathbf{P}\cdot\hat{\mathbf{e}})$ is reversed to $-(\mathbf{P}\cdot\hat{\mathbf{e}})$; the electric field at which this occurs is the coercive field $\mathcal{E}_c$. We present molecular dynamics (MD) simulations for a detailed investigation of polarization switching in $BaTiO_3$ through determination of (a) its temperature dependence, (b) paths followed during switching with field along different directions, and (c) detailed electric-field–temperature phase diagrams. This permits identification of different monoclinic phases that are stabilized as a function of electric field and temperature and are relevant to both ultrahigh piezoelectric response and polarization switching properties.

II. METHODS

We use a first-principles effective Hamiltonian H_{eff} in classical molecular dynamics simulations that (1) capture most nonlinearities by construction and (2) include thermal fluctuations in polarization and strain. A similar approach has been used earlier[12] in finding polarization paths as a function of applied field at a fixed temperature. In order to include effects of an external electric field on the system, a term $-Z^*\Sigma\mathcal{E}\cdot\mathbf{u}(\mathbf{R})$, where Z^* and $u(R)$ are the Born effective charge and displacement associated with the soft-mode variable of the unit cell at R, is added to H_{eff}. We use parameters in H_{eff} as determined in Refs. 13 and 14 from first-principles density functional theory calculations with local-density approximation (LDA). Use of LDA causes an underestimation of the lattice parameter; hence a negative pressure of -5 GPa is applied to all systems simulated[14] here.

Mixed space[15] MD is used here to determine finite temperature properties of H_{eff} with periodic boundary conditions. The FERAM code used in our simulations is described

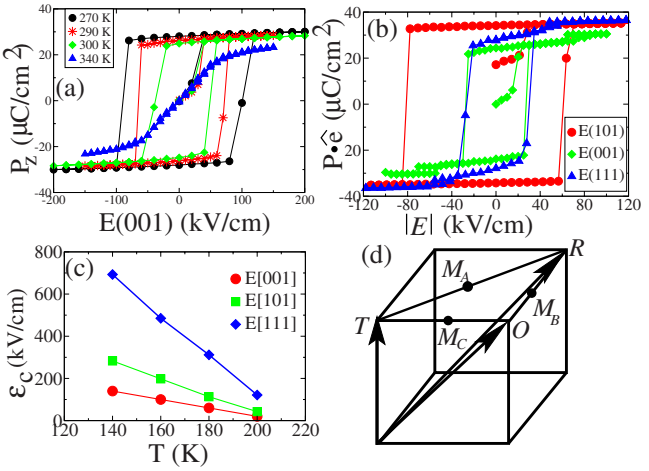

FIG. 1. (Color online) (a) Average value of polarization P_z as a function of electric field for cubic paraelectric (triangles) and tetragonal ferroelectric phases when electric field is applied along the [001] direction. (b) Hysteresis of $\mathbf{P}\cdot\hat{\mathbf{e}}$ in the orthorhombic phase as a function of $|E|$ for fields along (001), (101), and (111). (c) Coercive field $\mathcal{E}_c$ as a function of temperature for fields along (111), (101), and (001) directions, respectively, applied to rhombohedral phase. (d) Cohen's cube (Ref. 3).

in detail in Ref. 16 and the program can be downloaded from Ref. 17. In order to simulate polarization hysteresis, the temperature is first increased or decreased in steps of ~30 K to achieve an equilibrium at the temperature of the hysteresis simulation. Then, at fixed temperature, the electric field is switched on from zero to a positive value $E_{\max}$, from which it is decreased to $-E_{\max}$ in steps of about 10–100 kV/cm. Subsequently, it is again increased finally to $E_{\max}$ to obtain a complete hysteresis loop. At each temperature (and electric field), the system is thermalized for initial 70 000 time steps and then averaging is performed over the next 30 000 time steps amounting to a simulation period of 0.2 ns.

III. RESULTS

A. Polarization switching

For the high-temperature cubic paraelectric phase, we simulate the polarization response to electric field applied along the [001] direction. Our results [Fig. 1(a)] are fairly well described by the Langevin function $P(E)=L(E)=k_1[\coth\frac{k_2E}{k_BT}-\frac{k_BT}{k_2E}]$. As the temperature approaches the paraelectric-ferroelectric (tetragonal phase) transition $T_c(T\leftrightarrow C)$, (a) k_1, which relates to the saturated polarization remains roughly constant, while (b) k_2, which is proportional to the dielectric constant of the paraelectric phase, diverges. Almost perfect fits to $P(E)$ curves of the paraelectric phase with just two fitting parameters and their expected temperature dependence validate our MD simulations to further study these nonlinear hysteresis properties of the polar phases.

For polar phases, we simulate response to field applied (a) along the respective polar axis and (b) along other high-symmetry crystallographic directions (e.g., along the [101] direction of the tetragonal phase where **P** points along [001]). Generally, $\mathcal{E}_c$ reduces as the temperature increases up to the transition to higher-temperature phase [see results for tetragonal and rhombohedral phases in Figs. 1(a) and 1(c)]. We now focus on the direction dependence of polarization switching in orthorhombic and rhombohedral phases. In an orthorhombic phase, switching occurs at much lower fields when fields are along the [001] and [111] directions than along [101] [Fig. 1(b)]. Interestingly, with field applied along the [001] direction, an orthorhombic phase with **P**[110] initially transforms to another orthorhombic phase with **P**[101] [green (diamonds) curve, Fig. 1(b)]. In the rhombohedral phase, we find that the coercive field $\mathcal{E}_c$ when applied along the [001] direction is almost a factor of 5 smaller than the one when applied along the [111] direction [see Fig. 1(c)]. While the reduction in $\mathcal{E}_c$ with T can be readily understood through the concept of lowering of Landau free-energy barrier near the transition, a strong dependence of $\mathcal{E}_c$ on its direction is related to the fact that transition state itself depends on the field direction.

B. Polarization switching paths

In order to investigate the transition states relevant to switching, we examine the paths followed by the system during polarization switching. We use the following nomenclature to describe the different phases encountered along the polarization paths (Fig. 2): T (**P**[001]), O (**P**[101]), and R (**P**[111]) denote the tetragonal, orthorhombic, and rhombohedral phases, respectively, and M_A, M_B, and M_C denote the three different monoclinic phases as defined in Ref. 11. In the M_C phase, **P** points along $[0uv]$ $(u\neq v)$ and in the M_A and M_B phases, **P** points along $[uuv]$, with $u<v$ and $u>v$, respectively. The monoclinic phases are also illustrated with the Cohen's cube[3] [see Fig. 1(d)].

When E is parallel to **P**, the switching path is linear (from **P** to **−P**) by symmetry on the time scales (<2 ns) of our simulations. For fields not parallel to **P**, switching occurs typically as a two-step process, in which **P** first undergoes a rotation from a high symmetry to a monoclinic phase and then it reverses at $\mathcal{E}_c$. We focus here on switching paths in orthorhombic phase with fields along the (a) [001] and (b) [111] directions and in tetragonal phase with fields along the (c) [101] and (d) [111] directions (see Fig. 2).

In cases (a) and (c), switching paths are planar: polarization rotation corresponds to a jump from point 1 to point 2, where the initial O [Fig. 2(a)] and T [Fig. 2(c)] phases transform to the monoclinic phase M_C at 25 and $40\sqrt{2}$ kV/cm, respectively. These transformations are accompanied by a change in the slope of the eigenvalues η of the strain tensor as a function of electric field [Figs. 3(a) and 3(c)]. The sequence of phases, $O\rightarrow M_C\rightarrow T$ [Fig. 2(a)] and $T\rightarrow M_C\rightarrow O$ [Fig. 2(c)] can be readily rationalized through continuous paths on the Cohen's cube [see Fig. 1(d)]. Reversal of polarization occurs at $\mathcal{E}_c$'s 25 and $25\sqrt{2}$ kV/cm when $(\mathbf{P}\cdot\hat{\mathbf{e}})$ switches to $-(\mathbf{P}\cdot\hat{\mathbf{e}})$ corresponding to points 6 and 7 (as well as 9 and 10) in Fig. 2(a) [and green curve in Fig. 1(b)], and points 7 and 8 (and 13 and 2) in Fig. 2(c).

For cases (b) and (d), switching paths are nonplanar [see Table I for the points of rotation (**R**) and switching (**S**) on

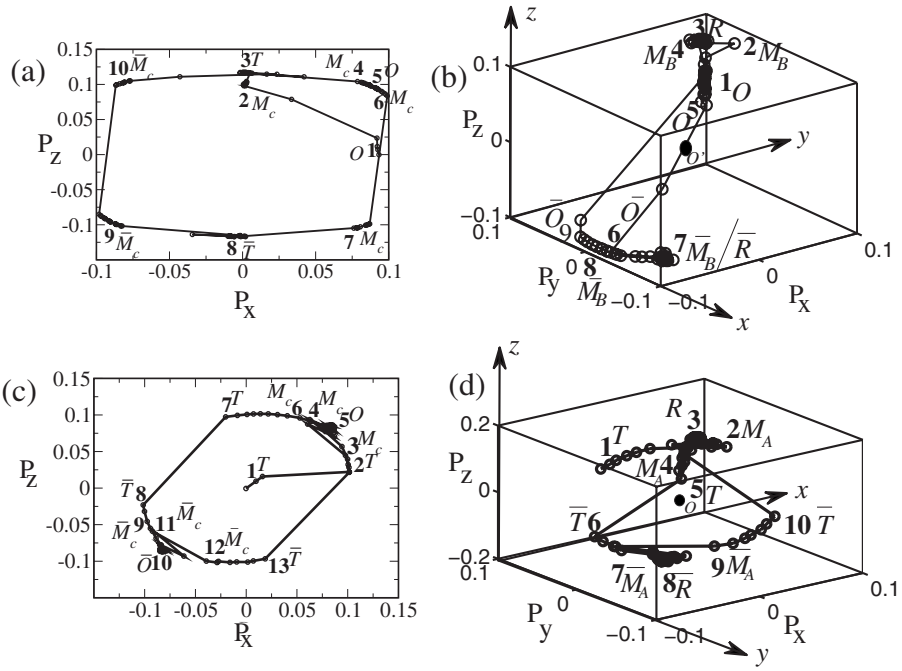

FIG. 2. Paths of polarization traced during switching when field is applied along the (a) [001] and (b) [111] directions to orthorhombic phase at 240 K and (c) [101] and (d) [111] directions to tetragonal phase at 290 K. The numbers mark the sequence of phases (nomenclature in the text) followed by **P**.

them]. **P** rotates from the initial *O* and *T* phases to monoclinic phases M_B and M_A at $15\sqrt{3}$ and $40\sqrt{3}$ kV/cm, respectively. These phase transformations manifest as changing slopes of η as a function of field [Figs. 3(b) and 3(d)]. A change in the slope of η at ~100 kV/cm signals a transformation from the monoclinic phases M_B and M_A to the rhombohedral phase when **P** aligns with the direction of the applied field. For *O* and *T* phases, at $\mathcal{E}_c$ equal to $15\sqrt{3}$ kV/cm, switching of polarization occurs as $(\mathbf{P}\cdot\hat{\mathbf{e}})$ reverses to $-(\mathbf{P}\cdot\hat{\mathbf{e}})$ corresponding to points 5 and 6 [see, Figs. 2(b) and 2(d) and Table I, and Fig. 1(b) for switching in the orthorhombic phase].

Thus, we find for the three ferroelectric phases of $BaTiO_3$ that switching with fields applied along polar direction occurs at much higher fields than that applied along other crystallographic directions. While the polarization rotation[3] through monoclinic phases (which are known to be present near the morphotropic phase boundaries[5,12,18]) has been shown to be responsible for giant piezoelectric response, we show that it also facilitates polarization switching at lower coercive fields and is crucial for memory applications.

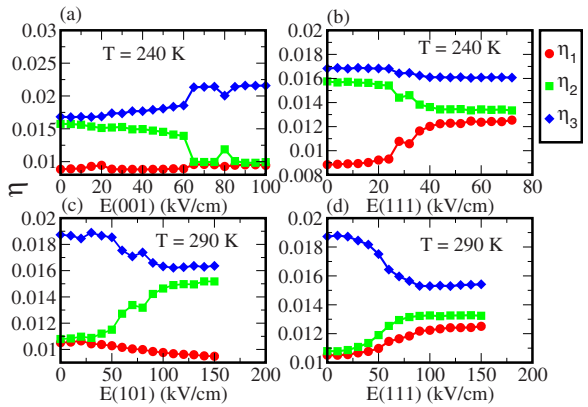

FIG. 3. (Color online) Eigenvalues η of strain tensor as a function of field applied along the (a) [001] and (b) [111] directions to the orthorhombic phase at 240 K and (c) [101] and (d) [111] directions to the tetragonal phase at 290 K.

C. Electric-field–temperature phase diagrams

We further investigate the existence and thermodynamic stability of monoclinic phases through *E-T* phase diagrams. We simulated temperature-dependent phase transitions for constant fields along the [001], [101], and [111] directions ranging from 10 to 100 kV/cm in steps of 5 kV/cm. The contour plots of eigenvalues of dielectric tensor as a function of field and temperature naturally give a picture of the electric-field–temperature (*E-T*) phase diagrams (Fig. 4). At zero electric field, dielectric response of $BaTiO_3$ exhibits (1)

TABLE I. Polarization and electric fields at important points along the polarization paths in (a) Fig. 2(b) and (b) Fig. 2(d). $\mathbf{R}_i$ denotes rotation and **S** denotes switching.

(a) Point, $E(111)$ (kV/cm)		(P_x, P_y, P_z) (μC/cm^2)	Phase
$\mathbf{R}_1$	1, 12.0	(24.1, 24.3, 3.3)	*O*
$\mathbf{R}_2$	2, 32.0	(23.2, 12.7, 23.0)	M_B
	3, 72.0	(21.4, 20.6, 21.4)	*R*
S	5, −12.0	(24.3, 23.7, −3.8)	*O*
	6, −20.0	(−24.0, −6.0, −24.1)	*O′*
(b) Point, $E(111)$ (kV/cm)		(P_x, P_y, P_z) (μC/cm^2)	Phase
$\mathbf{R}_1$	1, 10.0	(2.3, 26.3, 1.7)	*T*
$\mathbf{R}_2$	2, 70.0	(20.1, 14.1, 16.0)	M_A
	3, 140.0	(18.0, 19.1, 18.3)	*R*
S	5, −20.0	(−4.4, −6.1, 24.6)	*T′*
	6, −30.0	(−25.9, −5.5, −5.9)	*T″*

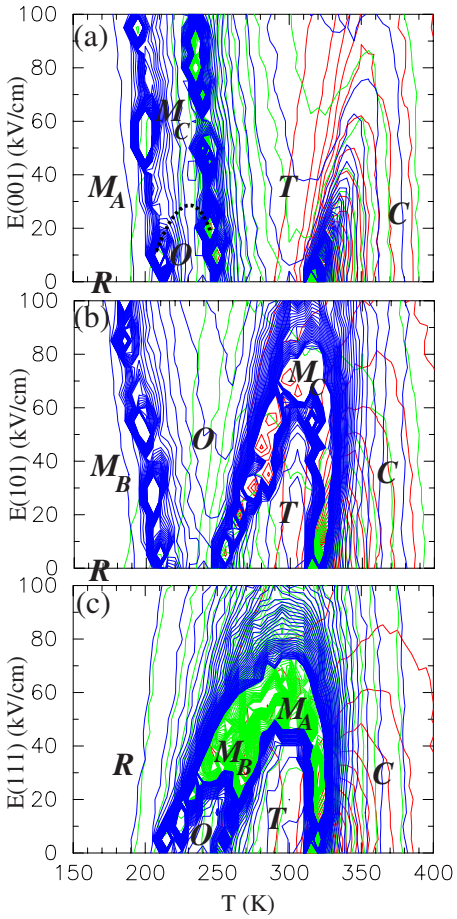

FIG. 4. (Color online) *E-T* phase diagrams for fields along the (a) [001], (b) [101], and (c) [111] directions expressed as contour plots of eigenvalues of the dielectric tensor. High density of contours near the peak values of dielectric response give rise to thick and dark lines which form the boundaries between different stable phases.

discontinuity and (2) sharp change at the phase transition, which become a bit smoother at nonzero electric fields. In the contour plots of eigenvalues of dielectric response in the *E-T* plane, these manifest through narrow regions of high density of contours. The width is about the numerical errors in transition temperatures or fields we estimate. Hence, these regions visible as dark thick curves, are interpreted here as phase boundaries.

For field along the [001] direction, there is no qualitative change in the phase transition behavior with increasing field [Fig. 4(a)]; the temperature range of the stable tetragonal phase expands with field. We note that a nonzero field breaks the symmetry of the system and the transition from *C* to *T* phase becomes diffused and above the field of 50 kV/cm, there is virtually no difference between the *T* and *C* phases. The orthorhombic phase transforms to monoclinic M_C phase above a field of about 30 kV/cm, as characterized by a change in the slope of strain as a function of electric field (see Fig. 3). When the field is applied along the [101] direction, the temperature interval of the stable orthorhombic phase expands with field. The tetragonal phase transforms through an intermediate monoclinic M_C phase to an orthorhombic phase above $80\sqrt{2}$ kV/cm. Boundaries of the region of stability of the M_C phase are characterized by peaks in eigenvalues of dielectric response appearing as thick dark lines [see Fig. 4(b)]. Similarly for field along the [111] direction, both tetragonal and orthorhombic phases transform at fields of about $40\sqrt{3}$ and $20\sqrt{3}$ kV/cm to M_A and M_B phases, respectively. Above the field of $60\sqrt{3}$ kV/cm, there is no clear boundary between rhombohedral and cubic phases. The lines of transition from monoclinic phases to *T*, *O*, and *R* phases (with increasing fields) in our *E-T* phase diagrams are topologically similar to those in Bell's work[10] based on phenomenological theory and even the fields of these transitions agree within ~20% with Bell's estimates. However, our phase diagram differs in an important way; the region of stable monoclinic phases appears only above nonzero electric fields and its boundary with *T*, *O*, and *R* phases at lower fields is characterized by (a) peak in the dielectric response (Fig. 4) and (b) change in the slope of η changes (Fig. 3), which reflects breaking symmetry beyond linear response of the zero-field phases. We note that the symmetry-breaking property is essentially a linear response of the system for small electric fields (less than 25 kV/cm). At higher fields the symmetry-breaking property arises partly from the change in the structure itself as reflected in the change in the slope (Fig. 3).

The sequence of phases appearing along the switching paths followed by the system during **P**-**E** hysteresis can be understood from the constant-temperature lines in the *E-T* phase diagrams. For example, applying field along the [111] direction of the tetragonal phase at 290 K would result in **P** tracing the path described in Fig. 2(d). The connectivity between different monoclinic phases and *T*, *O*, and *R* phases in the *E-T* phase diagram is consistent with that obtained from the Cohen's cube.[3] The change in the slope of strain as a function of field (see Fig. 3) at a crossover from a *T*, *O*, or *R* phase to a monoclinic one gives rise to the giant piezoelectric response arising at finite fields in experiments.[7,8]

IV. DISCUSSION AND SUMMARY

Switching fields obtained from our MD simulations are still much larger than the experimental estimates.[19] In a recent work published by us on epitaxial thin films sandwiched between electrodes,[20] it is observed that with increasing film thickness, coercive fields increase, contrary to the Kay-Dunn law. This was also found in earlier works[16,20,21] and is mainly because of two possible reasons: (i) switching is studied over short time scales in our simulations (less than nanosecond) and (ii) presence of defects is not accounted for (both of which facilitates inhomogeneous nucleation of domains[22–24] through which switching occurs in real materials). In the simulations here, switching occurs through a sort of homogeneous nucleation (see Fig. 5) in the presence of (a) electric field and (b) thermal fluctuations. Since our system size is small (about 6 nm in each direction), only a few domains are observed to form and grow; increasing the system size has a marginal impact on magnitudes of coercive fields (see Fig. 5); $\mathcal{E}_c$ of the tetragonal phase changes by 20 kV/cm when the applied field is along [001] at 290 K, while it changes by 4

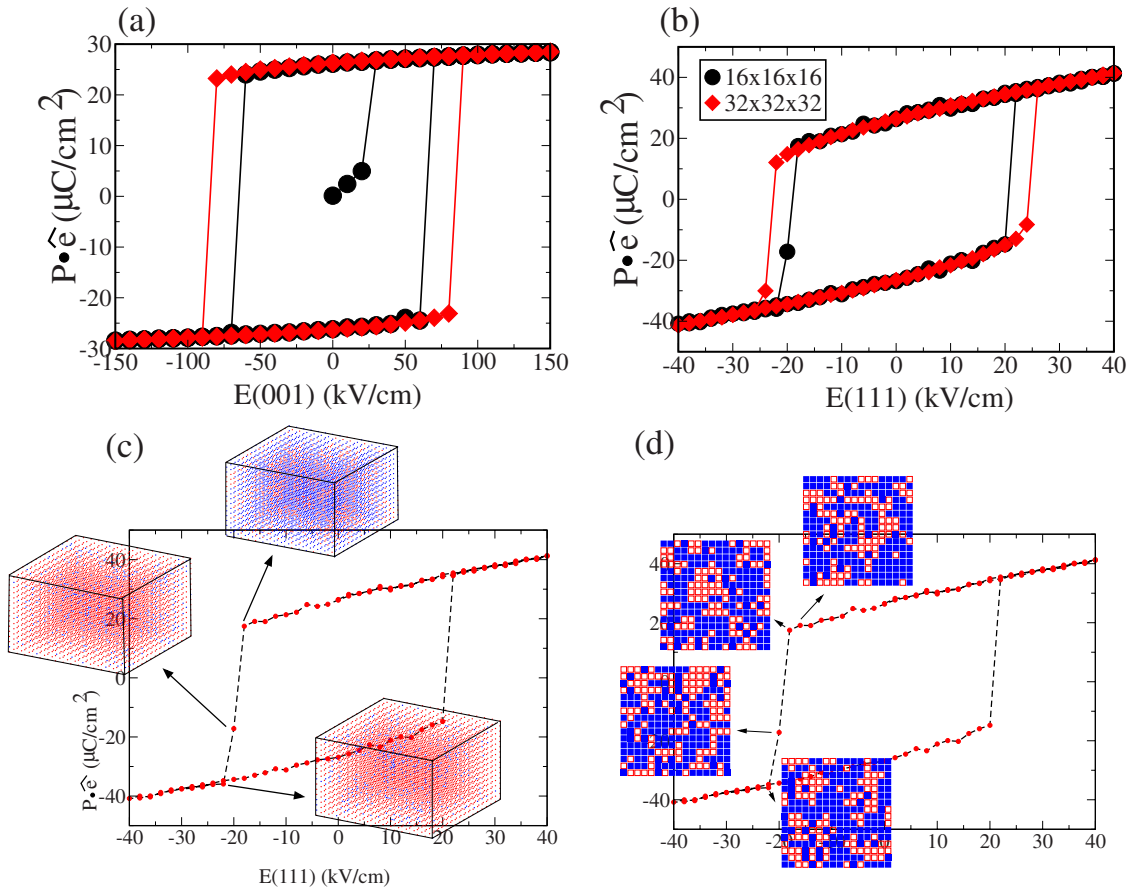

FIG. 5. (Color online) Hysteresis in $\mathbf{P}\cdot\hat{\mathbf{e}}$ when field is applied along the (a) [001] and (b) [111] directions of the tetragonal phase at 290 K for two system sizes, $16\times16\times16$ (black circles) and $32\times32\times32$ (red diamonds). (c) Three-dimensional view of polarization domains in snapshots at $E=-18$, -20, and -22 kV/cm; blue (dark) and red (light) dots correspond to $+\mathbf{P}\cdot\hat{\mathbf{e}}$ and $-\mathbf{P}\cdot\hat{\mathbf{e}}$, respectively. (d) Horizontal cross section (xy plane) where $+z$ and $-z$ polarized sites are symbolized by empty and filled boxes, respectively, for $16\times16\times16$ system showing the presence of domains.

kV/cm when applied along the [111] direction, as the system size is doubled from $16\times16\times16$ to $32\times32\times32$. We note that a stronger size dependence in the former is probably due to its greater energy barrier of switching.

Landauer[25] observed from Landau-Devonshire mean-field theories (where thermal fluctuations are absent) that energy barriers estimated for nucleation of reversely polarized domains are $10^3 k_B T$ (Refs. 22 and 25) at fields of about 100 kV/cm. We show that this barrier is considerably reduced when the thermal fluctuations are treated correctly, facilitating switching to occur at lower coercive fields (20–60 kV/cm depending on temperature in comparison to 200 kV/cm estimated from Landau theory[25]). The fact that observed $\mathcal{E}_c$'s in experiments are still lower is believed to be because of the heterogeneous nucleation of domains.[24]

Formation of a new domain with opposite polarization at fields labeled with **S** in Table I (which correspond to fields just before the system "switches" marked by discontinuities in the hysteresis loops) is driven by thermal fluctuations. An interesting concept emerging from our study is that the rotation of the polarization vector through intermediate monoclinic phases which appear prior to switching (see the polarization path diagrams, Fig. 2) enables switching to occur at lower coercive fields (see Table I). The monoclinic phases also appear in the electric-field–temperature phase diagrams with increasing electric-field magnitudes (Fig. 4).

To summarize, we have used effective Hamiltonian in molecular dynamics simulations and have shown that (1) switching fields are highest for the cases when the external electric field is applied along the direction of the polar axis and (2) switching occurs at low values of fields along other directions due to the polarization rotation through monoclinic phases. Stability of these monoclinic phases has been carefully analyzed through determination of the E-T phase diagrams, which should be fundamental to the design of both electromechanical and memory type of devices.

ACKNOWLEDGMENTS

J.P. thanks CSIR and T.N. thanks JNCASR, MEXT Japan, and JSPS. We acknowledge helpful discussions with Dhananjai Pandey and Subir K Das. We thank the CCMS supercomputing facility at JNCASR.

[1] M. Dawber, K. M. Rabe, and J. F. Scott, Rev. Mod. Phys. **77**, 1083 (2005).
[2] J. F. Scott and C. A. P. de Araujo, Science **246**, 1400 (1989).
[3] H. Fu and R. E. Cohen, Nature (London) **403**, 281 (2000).
[4] S.-E. Park and T. R. Shrout, J. Appl. Phys. **82**, 1804 (1997).
[5] B. Noheda, D. E. Cox, G. Shirane, S.-E. Park, L. E. Cross, and Z. Zhong, Phys. Rev. Lett. **86**, 3891 (2001).
[6] S. K. Mishra, D. Pandey, and A. P. Singh, Appl. Phys. Lett. **69**, 1707 (1996).
[7] S. Wada, S. Suzuki, T. Noma, T. Suzuki, M. Osada, M. Kakihana, S.-E. Park, L. E. Cross, and T. R. Shrout, Jpn. J. Appl. Phys., Part 1 **38**, 5505 (1999).
[8] S.-E. Park, S. Wada, L. E. Cross, and T. R. Shrout, J. Appl. Phys. **86**, 2746 (1999).
[9] D.-S. Paik, S.-E. Park, S. Wada, S.-F. Liu, and T. R. Shrout, J. Appl. Phys. **85**, 1080 (1999).
[10] A. J. Bell, J. Appl. Phys. **89**, 3907 (2001).
[11] D. Vanderbilt and M. H. Cohen, Phys. Rev. B **63**, 094108 (2001).
[12] L. Bellaiche, A. Garcia, and D. Vanderbilt, Phys. Rev. B **64**, 060103(R) (2001).
[13] W. Zhong, D. Vanderbilt, and K. M. Rabe, Phys. Rev. Lett. **73**, 1861 (1994).
[14] W. Zhong, D. Vanderbilt, and K. M. Rabe, Phys. Rev. B **52**, 6301 (1995).
[15] B. P. Burton, E. J. Cockayne, and U. V. Waghmare, Phys. Rev. B **72**, 064113 (2005).
[16] T. Nishimatsu, U. V. Waghmare, Y. Kawazoe, and D. Vanderbilt, Phys. Rev. B **78**, 104104 (2008).
[17] http://loto.sourceforge.net/feram/
[18] B. Noheda, Z. Zhong, D. E. Cox, G. Shirane, S.-E. Park, and P. Rehrig, Phys. Rev. B **65**, 224101 (2002).
[19] B. Jaffe, W. R. Cook, Jr., and H. Jaffe, *Piezoelectric Ceramics* (Academic, London, 1971), p. 78.
[20] J. Paul, T. Nishimatsu, Y. Kawazoe, and U. V. Waghmare, Appl. Phys. Lett. **93**, 242905 (2008).
[21] E. B. Tadmor, U. V. Waghmare, G. S. Smith, and E. Kaxiras, Acta Mater. **50**, 2989 (2002).
[22] A. M. Bratkovsky and A. P. Levanyuk, Phys. Rev. Lett. **85**, 4614 (2000).
[23] O. Trithaveesak, J. Schubert, and Ch. Buchal, J. Appl. Phys. **98**, 114101 (2005).
[24] P. Chandra, M. Dawber, P. B. Littlewood, and J. F. Scott, arXiv:cond-mat/0206014 (unpublished).
[25] R. Landauer, J. Appl. Phys. **28**, 227 (1957).